Near-Inertial Wave Propagation into the Pycnocline during Ocean Storms: Observations and Model Comparison

MURRAY D. LEVINE AND VASSILIS ZERVAKIS

College of Oceanic and Atmospheric Sciences, Oregon State University, Corvallis, Oregon

(Manuscript received 5 April 1994, in final form 11 November 1994)

ABSTRACT

Observations of near-inertial oscillations collected during the Ocean Storms Experiment in the northeast Pacific Ocean are compared with results from a linear, numerical model on a β plane, developed by Zervakis and Levine. A slab mixed layer model, forced by the observed wind time series, is used to identify three isolated events of local generation in October, January, and March for detailed analysis. Synoptic storm track maps are used to estimate the initial horizontal wavenumber of the mixed layer currents that are used as initial conditions to the model. A comparison of the model with the observed currents reveals some differences and similarities. Overall the January and March events are better represented by the model than the October event. The timescale of the initiation of vertical propagation of energy from the mixed layer occurs almost immediately in October rather than after 8 days in January and March—this difference cannot be explained by the model. The observed vertical and temporal structure indicates that the near-inertial energy propagated as a "beam" of energy through the pycnocline, especially in October. In the model the wave energy appears to accumulate at the top of the pycnocline. Physical processes that might be responsible for the deficiency of the model are discussed.

1. Introduction

Near-inertial oscillations are a common feature of the upper ocean. These oscillations are usually wind driven, occuring after the passage of storms. The inertial frequency f is a natural frequency of the ocean—the transfer function between surface forcing and mixed layer response peaks at f. A significant fraction of this mixed layer energy radiates into the pycnocline in the form of near-inertial internal gravity waves. This process may constitute a major link of kinetic energy and momentum transfer from the atmosphere to the deeper ocean.

The purpose of this paper is to present observations of the propagation of near-inertial waves made during the Ocean Storms Experiment in the northeast Pacific Ocean and to compare these observations with results from a linear model. The near-inertial response to three isolated storm events are analyzed in detail using data from a vertical array of instruments. An unforced, linear numerical model on a β plane, developed in Zervakis and Levine (1995, hereafter ZL), is used as a framework for understanding the vertical and horizontal propagation of energy into the pycnocline. Here, we adopt a simplified view of the generation process and assume that the mixed layer responds to the wind stress as a solid slab (Pollard and Millard 1970). The focus of this paper is to understand the subsequent decay of energy due to the radiation of near-inertial waves into the pycnocline. Similarities between the data and model are identified; differences are explored to help illuminate failures in our idealized view of the propagation of these motions.

The decay of near-inertial motion is perhaps less well understood than the generation. After a storm the mixed layer currents decay over a period ranging from days to weeks. A number of processes have been proposed as sinks of that energy. Near-inertial waves can generate high vertical shear, thus creating turbulence that could be a major factor in dissipating the wave field (Eriksen 1991; Hebert and Moum 1994). Broutman and Young (1986) and Henyey et al. (1986) have shown that high-frequency internal waves can extract energy from near-inertial waves by nonlinear transfer. Bell (1978) proposed a process of generation of high-frequency, high-wavenumber internal waves by the advection of undulations of the mixed layer over a stratified ocean, with the undulations created by turbulent eddies or Langmuir circulation.

However, most investigations have focused on the radiation of near-inertial waves as the primary process for extracting energy from mixed layer oscillations—a process often called inertial pumping. A finite horizontal scale in the structure of the mixed

Corresponding author address: Dr. Murray D. Levine, College of Oceanic and Atmospheric Sciences, Oregon State University, Oceanography Adm. Bldg. 104, Corvallis, OR 97331-5503.
E-mail: levine@oce.orst.edu

layer current is necessary for inertial pumping to occur. Horizontal velocity gradients cause convergences and divergences that vertically displace the base of the mixed layer; the resulting pressure gradients generate internal waves in a process that might also be described as time-dependent Ekman pumping. A multitude of models have been used to describe this process. For example, Pollard (1970) and Kundu and Thomson (1985) have advected idealized wind stress distributions over the ocean surface in a linear model using vertical normal modes. Geisler (1970) modeled the response of a two-layer ocean to a hurricane. Rubenstein (1983) used a multilayered model with eddy diffusivity and bottom porosity; Price (1983) also used a multilayered ocean and looked at the response to hurricanes. Greatbatch (1983, 1984) included nonlinear dynamics and investigated the effect of entrainment. Kundu (1986) included the presence of a coast, using vertical modes with a vertical eddy diffusivity. Shay and Elsberry (1987) and Shay et al. (1989) concentrated on oceanic response to hurricanes. D'Asaro (1989) examined the role of the β effect in modifying the meridional scale of the waves and thereby setting the timescale of the vertical propagation of energy from the mixed layer. Recently, Kundu (1993) has explored the consequences of the β plane on internal waves generated by a traveling wind field. In this paper we choose to use a linear model on a β plane (ZL) modified from Gill (1984, hereafter G84) that tracks the propagation of waves resulting from a given initial condition in the mixed layer. The model results are then a function of the specified initial horizontal structure of the oscillations in the mixed layer. Estimates of the velocity of storm tracks from synoptic weather maps are used to calculate the initial horizontal scale in the mixed layer.

There have been limited comparisons between open-ocean inertial currents and model results. Price (1983) compared observations of inertial currents in the wake of a hurricane with a model on a constant f plane and found good agreement. Other comparisons of model results with data at the relatively short horizontal scales of hurricanes (Shay and Elsberry 1987; Shay et al. 1989) were also quite satisfactory. There have been relatively few detailed model and data comparisons of large-scale, near-inertial responses forced by the advection of large atmospheric fronts (e.g., Krauss 1981; Millot and Crépon 1981; De Young and Tang 1990). The extensive data gathered during Ocean Storms has provided many investigators an opportunity for detailed comparison between theory and observations that should noticeably increase our understanding of near-inertial wave propagation (D'Asaro et al. 1995).

The Ocean Storms observations used in this paper are described in section 2. Section 3 describes the wind-forced slab model that was used to identify three events of local generation chosen for further analysis. A short description of the numerical model developed in ZL is presented in section 4. The Ocean Storms observations are compared with the numerical model results in section 5. A summary and conclusions are given in section 6.

2. Observations

a. The C1 mooring

The following analysis is based primarily on data collected from a single mooring deployed in the northeast Pacific from August 1987 to June 1988 as a part of the Ocean Storms Experiment. The mooring was positioned at 47°25.4′N, 139°17.8′W (C1), in water 4225 m deep in an area far from major topographic features; the local bathymetry can be considered level for all practical purposes. The mooring contained seven vector measuring current meters (VMCM; Interocean) in the upper ocean at 60, 80, 100, 120, 140, 160, and 195 m and five Aanderaa (RCM-5) current meters in the deep ocean at 500, 1000, 2000, 3000, and 4000 m. The sampling rate was 15 minutes for the VMCMs and 1 hour for the Aanderaas. In addition to current speed and direction the current meters recorded temperature. Five Seacats (Sea-Bird Electronics) measured temperature and conductivity at 70, 89, 109, 128, and 150 m. The two shallowest Seacats were also equipped with Digiquartz pressure sensors (Paroscientific) to monitor mooring motion. Three Aanderaa thermistor chains (TR-1) covered the depth ranges 206–236, 250–260, and 375–425 m, sampling every two hours.

b. Supporting measurements

Other relevant meteorological and oceanographic measurements were made near the mooring by other investigators. A time series of wind velocity was recorded at the C0 mooring, 18 km northwest of C1, deployed by R. Davis (Scripps Institution of Oceanography) (Large and Crawford 1995). The anemometer was located at a height of 4 m, and the wind stress at the sea surface was estimated assuming a neutrally stratified atmosphere (Smith 1988) (Fig. 1a).

Additional meteorological observations from ships of opportunity, the P-3 Orion aircraft, permanent NOAA buoys, other Ocean Storms moorings, and Argos-tracked surface drifters, were compiled and combined with synoptic weather maps by Lindsay (1988). The most intense sampling was in the period from September to December 1987.

The evolution of the mixed layer depth was tracked with an Aanderaa thermistor chain (TR-1) that was attached on the W mooring located 50 km to the west of C1 (Fig. 1c). The chain consisted of thermistors at 10-m intervals between 9 and 109 m from the surface. We used the temperature measured at W because the shal-

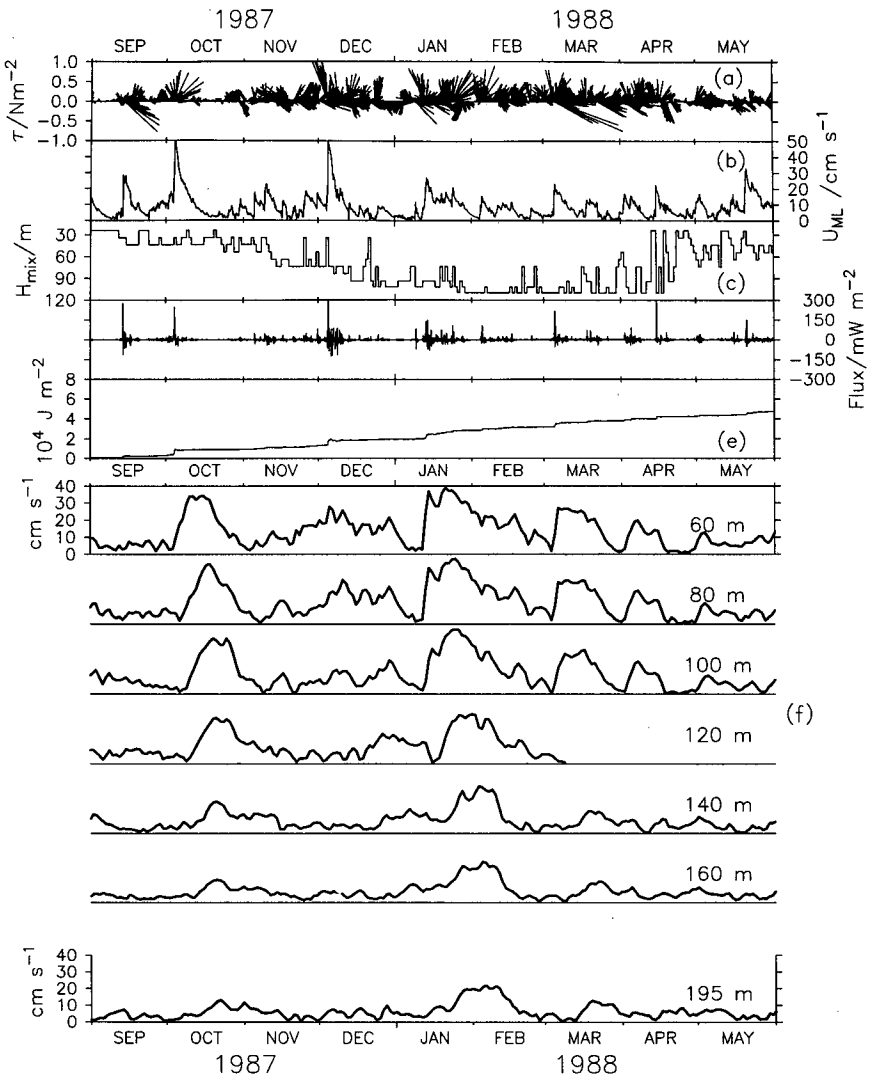

FIG. 1. (a) Wind stress estimated from anemometer on C0; (b) modeled amplitude of mixed layer inertial currents (slab model); (c) observed mixed layer depth; (d) modeled energy flux into the mixed layer from the wind (slab model); (e) modeled cumulative energy input into the mixed layer from the wind calculated by integrating the flux (d); (f) observed amplitude of near-inertial oscillations at 60, 80, 100, 120, 140, 160, and 195 m.

lowest sensor on C1 was located at 60 m, which remained below the mixed layer until mid-November. After November an intercomparison reveals that the base of the mixed layer was at the same depth at W and C1 (Levine et al. 1990).

Profiles of buoyancy frequency N were calculated for the top 500 m using CTD casts from two cruises in 1987 of the CSS *Parizeau* from September to December (Tabata 1988). The N profiles were extended to the ocean bottom using historical data (Levitus 1982). To approximate the time-varying stratification, the measured mixed layer depths were incorporated into the N profiles.

c. *Complex demodulation*

The technique of complex demodulation (e.g., Koopmans 1974) was combined with rotary decomposition (Gonella 1972) to separate the near-inertial signal $\mathbf{U}_-$ (clockwise rotating component) from the noise $\mathbf{U}_+$ (counterclockwise rotating component). Both $\mathbf{U}_+$ and $\mathbf{U}_-$ are vectors having amplitude and phase information. The decomposition was done over 64-h sections in order to separate the local inertial peak (at 0.0614 cph) from the semidiurnal tidal band (0.08–0.083 cph). Since the local inertial period is not an even multiple of the sampling intervals

of the current meters, we chose a demodulation frequency $\omega_0 = 0.0625$ cph that is very near the inertial frequency. The width of the main lobe of the response of the filter (0.0312 cph) is sufficient to include the local inertial frequency without significant loss of spectral power (Fig. 2). The demodulation was applied every 32 hours, resulting in a 50% data overlap.

The frequency can be estimated from the slope in time of the demodulated phase. It is clearest to reference the phase to the local f. Then the phase of a perfectly inertial current would result in a line parallel to the time axis; a frequency higher than f would have a positive slope.

Theoretical considerations require resolving frequency differences of $0.01f$. To achieve this resolution, conventional Fourier transform analysis would require record lengths on the order of 100 inertial periods. Then much of the information about individual events would be lost. But complex demodulation allows us to track these frequencies using record lengths of only a few inertial periods. The principles of time series analysis are not violated; the frequency resolution is the same for both a complex demodulation filter and a conventional Fourier transform. However, by assuming that each spectral band represents a single wave, complex demodulation can be used to estimate the time-varying amplitude and phase of the wave. The change of the phase with time is then an accurate estimate of the frequency under the single wave assumption.

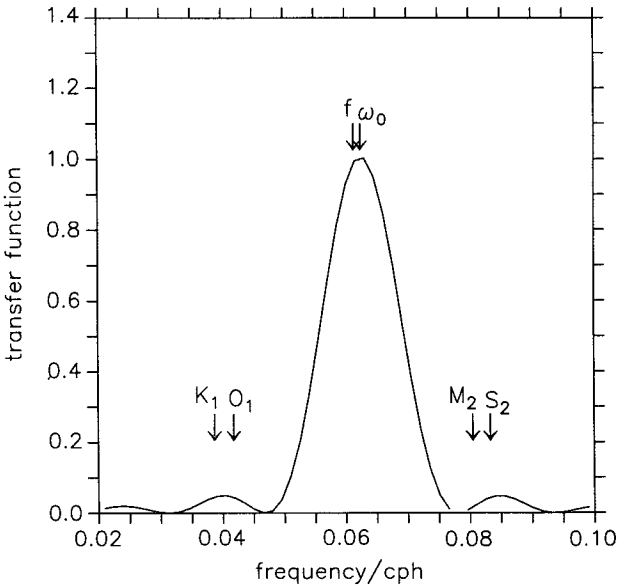

FIG. 2. The transfer function for the complex-demodulation filter. The demodulation is centered around $\omega_0 = 0.0625$ cph. The local inertial frequency f at 47.5°N and dominant tidal frequencies are indicated.

d. Near-inertial currents

The observed amplitudes of the near-inertial currents for the entire time series from 60 to 195 m depth are plotted in Fig. 1f. In general, the currents decrease in magnitude with depth, suggesting generation at the surface. For a number of events the waves appear to propagate downward slowly as "packets" on timescales of days. Currents in the mixed layer are vertically homogeneous. Note that no instruments were in the mixed layer until mid-November (Fig. 1c).

3. The slab mixed layer model

The near-inertial wave field observed in the ocean is a sum of waves generated locally and waves that have radiated from distant sources. In the analysis of observations at Ocean Storms it is important to make that distinction. The slab mixed layer model (Pollard and Millard 1970) provides a valuable tool for that purpose. The model requires only a time series of wind stress and mixed layer depth H_{mix} to provide a first-order description of the local mixed layer response to wind forcing. The model assumes that the wind stress is distributed uniformly over a horizontally infinite, homogeneous surface layer of constant thickness H_{mix}. Since the mixed layer is assumed to be unstratified, the only natural frequency of the system is f. Having assumed horizontal homogeneity, there are no horizontal pressure gradients to cause inertial pumping, which would lead to the vertical propagation of energy out of the mixed layer. Hence, except for destructive interference by other storm events, there is no mechanism for the decay of the inertial oscillations. To compensate, Pollard and Millard (1970) introduced a body (Rayleigh) friction term, so that the oscillations are damped exponentially in time; a typical e-folding time of 4 days is used here. Since its introduction, the model has been used by many investigators to simulate the near-inertial response of the mixed layer to local wind forcing (e.g., Paduan et al. 1988; D'Asaro 1989).

The results of the slab model using the wind stress and H_{mix} observed at Ocean Storms are shown in Fig. 1. The results are displayed as in D'Asaro (1989) showing the speed of the inertial response in the mixed layer (Fig. 1b), the energy flux into the mixed layer (Fig. 1d), and its integral in time (Fig. 1e). The model predicts several strong isolated generation events, especially the three starting on 4 October, 13 January, and 5 March that will be the focus of this paper. Each of these events is displayed on an expanded scale in Figs. 3, 4, and 5. [For an analysis of the response to the complicated storms in November and December, see D'Asaro (1995).]

The model shows that the sudden strong wind event of 4 October forced large inertial oscillations in the mixed layer, increasing the energy abruptly by 5000

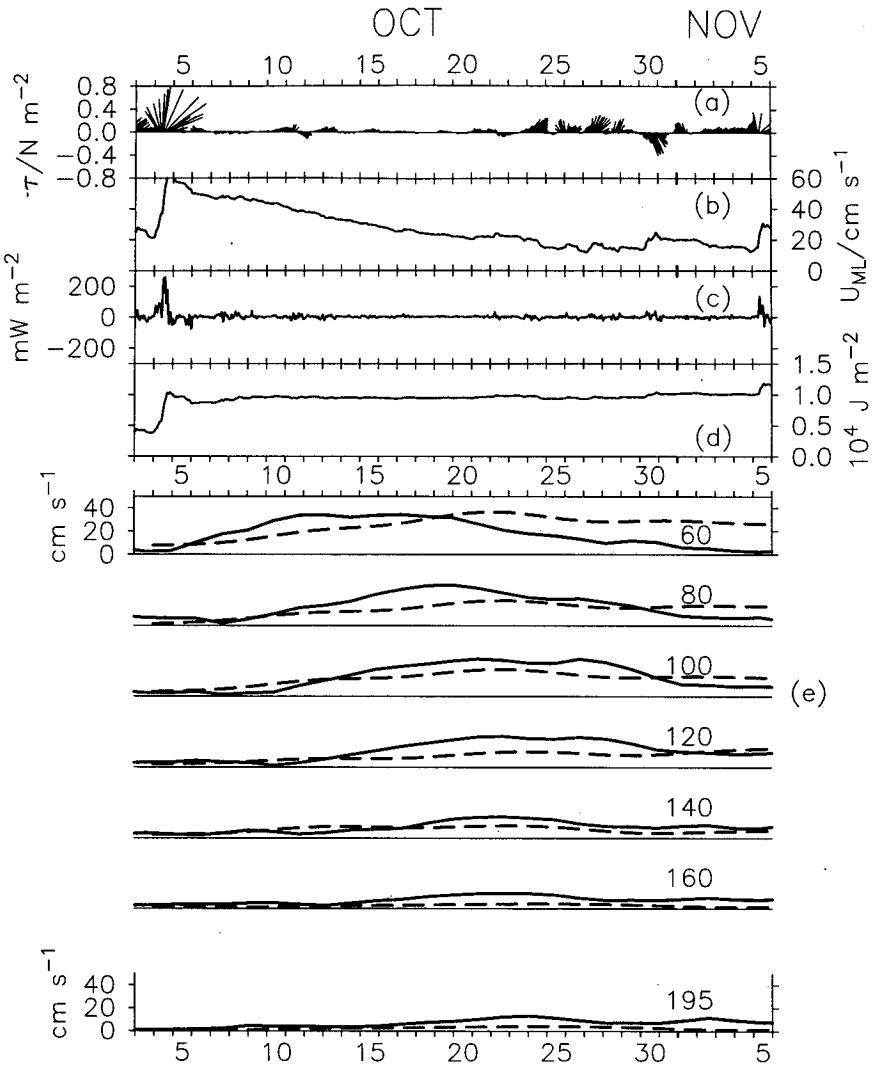

FIG. 3. October event displayed as in Fig. 1 on an expanded scale. (a) Wind stress estimated from anemometer on C0; (b) modeled amplitude of mixed layer inertial currents (slab model); (c) modeled energy flux into the mixed layer from the wind (slab model); (d) modeled cumulative energy input into the mixed layer (slab model); (e) observed (solid) and modeled (dashed) amplitude of near-inertial oscillations at 60, 80, 100, 120, 140, 160, and 195 m.

J m^{-2} (Fig. 3d). This event is an ideal candidate for study as no additional significant forcing occurred for 25 days.

The event beginning on 12 January follows a short period of exceptionally weak currents, but is not as isolated as the October storm (Fig. 4). From 13 through 26 January and then again starting on 4 February there were a series of forcing events that affected the mixed layer oscillations. Looking in detail at the slab model, the 13 January storm infused about 5000 J m^{-2} of kinetic energy into the mixed layer (Fig. 4d). Then the series of storms from 17 to 24 January slowly added another 5000 J m^{-2} into the mixed layer. The observations in the mixed layer at 60 and 80 m generally follow the slab model result (Fig. 4e).

A note of caution regarding the slab model results after 13 January. The slab model solution is constructed by adding the response of each successive event. Hence, slight variations in the phase of preexisting oscillations will significantly affect how the energy is added, constructively or destructively. The slab model assumes that frequency at a fixed location does not vary in time, but on a more realistic β plane the frequency will vary. A close look at the mixed layer observations after 13 January shows a decay of the inertial oscillation amplitude by ~8 cm s^{-1} (corresponding to a de-

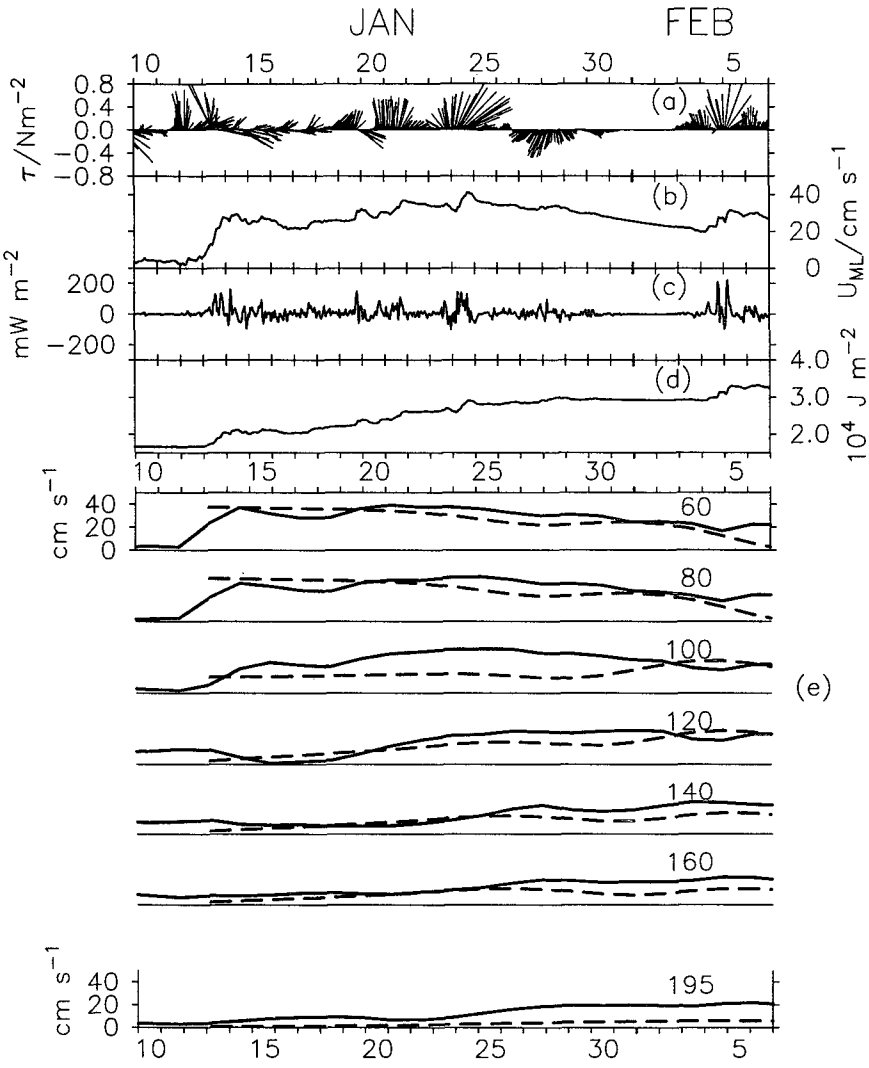

FIG. 4. As in Fig. 3 but for the January event.

crease in mixed layer horizontal kinetic energy (HKE) of 3000 J m^{-2}) to 17 January. This decrease is followed by an amplitude increase of ~13 cm s^{-1} (an HKE increase of 5000 J m^{-2}) over the next few days. Inspection of the corresponding mixed layer phase observations (next section) does not reveal any significant phase jump, suggesting that the additional forcing on those days was nearly either in or out of phase. Here we will only model the response to the single event of 13 January—a more accurate modeling of the January event would require consideration of multiple forcing events.

Although March 1988 was quite a windy month, the slab model indicates that only the event of 5 March generated considerable inertial oscillations (Fig. 5), adding about 4000 J m^{-2} to the mixed layer. Another, weaker event on 18 March added less than 1000 J m^{-2} into the mixed-layer.

On 2 April, there is an increase in the observed inertial currents, homogeneous from 60 to 100 m, as predicted by the slab model. Since H_{mix} is quite variable and often less than 60 m in April (restratification period), we cannot directly compare the modeled mixed layer currents with the currents observed at 60 m. The model also predicts accurately the generation of inertial currents on 1 May. Note that on May 1 the observed mixed layer depth is 40–60 m, while the current meter response is nearly uniform to a depth of more than 100 m. The model predicts a response on 18 May that is not found in the data. Lacking detailed stratification profiles, we defer modeling the April and May events.

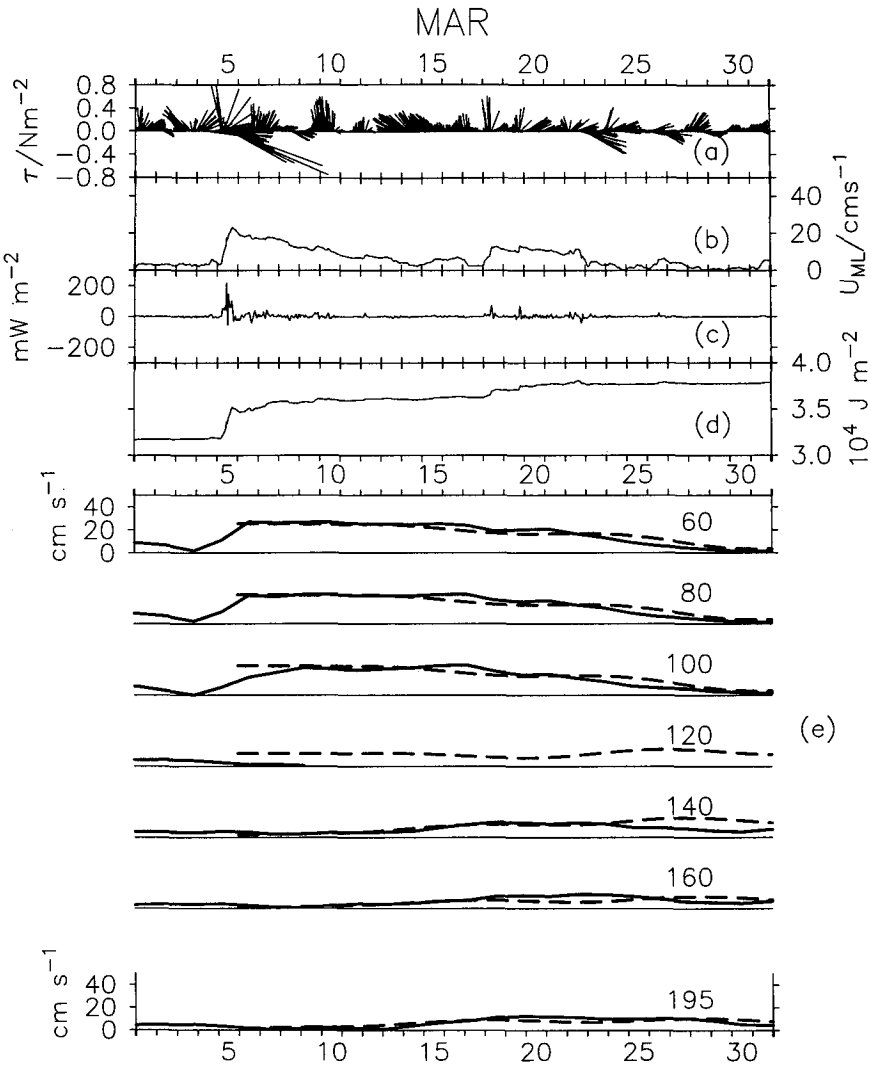

FIG. 5. As in Fig. 3 but for the March event.

The near-inertial response observed during Ocean Storms was compared with the 10-yr climatology calculated by D'Asaro (1985) for Ocean Weather Station P (50°N, 145°W). Both the October and March events can be considered typical of North Pacific fronts, each injecting about 5000 J m^{-2} of kinetic energy into the mixed layer, with impulses of energy fluxes of the order of 100 mW m^{-2}. The fall period (Oct–Dec 1987) had an average kinetic energy flux of 0.95 mW m^{-2}—less than the climatological average for this period of about 3 mW m^{-2}. The winter period (Jan–Mar 1988) average flux of 2.2 mW m^{-2} was near the climatological average of about 1.8 mW m^{-2}. Overall the average observed energy flux from September to May (Fig. 1) was 1.9 mW m^{-2}. D'Asaro (1985) estimated the average flux from September to March to be ~2.0–2.5 mW m^{-2}. So, the near-inertial forcing during the Ocean Storms Experiment appears to have been typical.

4. Numerical model

a. Description

The observed propagation of near-inertial energy at Ocean Storms is studied in the context of the numerical model presented in ZL. This model, patterned after G84, is not directly forced by the wind stress, but is set in motion by the initial conditions. The model then tracks the horizontal and vertical propagation of near-inertial waves that result from the initial disturbance. The model uses linear dynamics on a β plane. The solution is expanded with vertical modes in depth and Fourier transforms in x (zonal). The propagation of

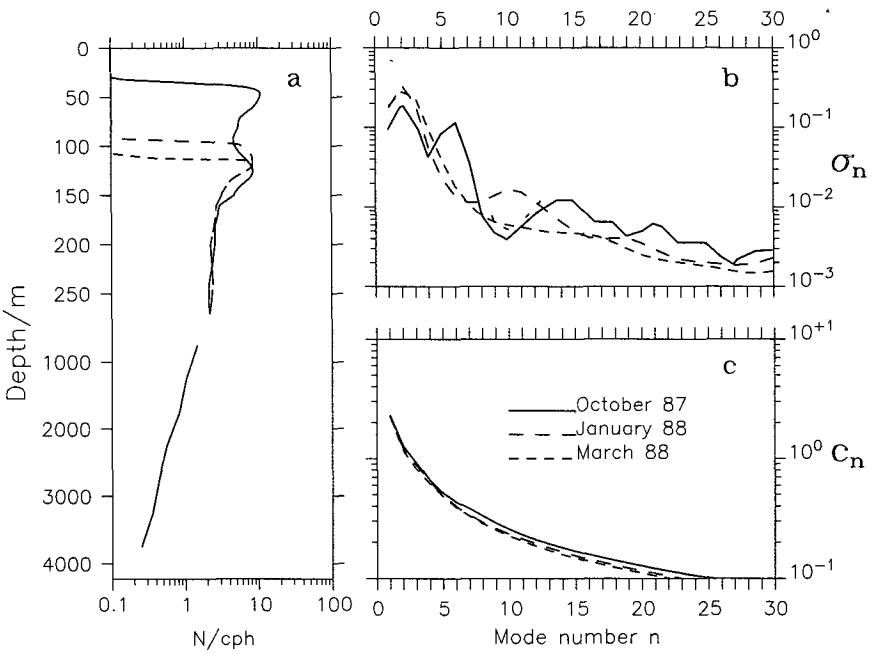

FIG. 6. (a) The N profiles used in the model for the three events. The relative weights of the modes σ_n (b) and the corresponding modal eigenspeeds c_n (c) are shown as a function of mode number for all three events.

each mode is solved numerically using finite differences in both y (meridional) and time.

We assume the initial condition in the mixed layer is set by the passage of a fast-moving atmospheric front; below the mixed layer there is no motion initially. The oceanic response to a moving front can be described separately for each vertical mode as a function of the advection speed C of the front and the *eigenspeed* c_n of the mode (Gill 1982; chapter 9.11). In this analysis we assume that the storms are relatively "fast"; that is, $C > c_n$. The equations are then hyperbolic for all modes, and the solution is a wake of near-inertial oscillations propagating behind the forcing. The mixed layer response occurs at a horizontal wavenumber $\kappa = f/C$ and is consistent with a near-inertial wave propagating in the direction of the storm track. Note that the quantity $2\pi/\kappa$ is called the "inertial wavelength" by Kundu and Thomson (1985), while D'Asaro (1989) calls $1/\kappa$ the "advection scale" of the storm.

The behavior of the numerical model is determined by the initial conditions. We consider an initial disturbance dominated by a single horizontal wavenumber of finite horizontal extent. We assume the horizontal pattern of the initial current is consistent with a fast moving front; this differs from the initial condition used by G84. A thorough discussion of the model as a function of initial conditions is presented in ZL; some of the results of this study are summarized below.

The initial vertical structure of uniform velocity in the mixed layer and zero velocity below is satisfied by the summation of vertical modes. Following the normalization of G84, we define σ_n as the fractional contribution of each mode to the initial velocity profile. The values of σ_n depend on $N(z)$ and sum to 1. It can be shown that σ_n also represents the fractional contribution of each mode to the kinetic energy of the whole water column (G84). The various $N(z)$ profiles used in calculating the mode shapes are shown in Fig. 6a. The modal coefficients σ_n and the modal eigenspeeds c_n are also shown as a function of mode number (Figs. 6b,c). Note that σ_n for the low modes are smaller in October when the mixed layer is shallower than in January and March. The eigenspeeds of the modes, however, do not vary significantly among the profiles.

After $t = 0$, each mode begins to propagate horizontally and to oscillate at a different frequency. The frequency is related to the horizontal wavenumber and eigenspeed by the dispersion relation for mode n given by

$$\omega_n^2 = f^2 + c_n^2(k^2 + l^2). \tag{1}$$

Lower modes oscillate at a higher frequency since c_n is larger. On a β plane the local frequency is not constant in time since the local meridional wavenumber varies in time as

$$l(t) = l_0 - \beta t \tag{2}$$

TABLE 1. The velocity of the fronts responsible for the three events estimated from storm track maps (Lindsay 1988). Estimated horizontal scale, wavenumber, and wavelength of the mixed layer currents generated by these fronts are also given.

Event	Compass bearing (0° = N) (deg)	Speed (m s^{-1})	k_0^{-1} (km)	l_0^{-1} (km)	k_0 [10^{-3} (km)$^{-1}$]	l_0 [10^{-3} (km)$^{-1}$]	Wavelength (km)
4 Oct	30	16	290	165	3.5	6.1	900
12 Jan	45	10	126	122	7.9	8.2	550
3 Mar	60	15	161	262	6.2	3.8	862

(e.g., D'Asaro 1989). For typical values of initial wavenumber l_0 (corresponding to fast moving fronts), the term βt soon becomes large and $|l(t)|$ increases. Therefore, due to dispersion, the frequency of each mode eventually increases locally in time.

b. *Modal interference (beating)*

Vertical propagation of energy in the model can be explained somewhat as the consequence of the beating of modes, since each mode oscillates at a different frequency (G84). After $t = 0$ the sum of the modes will no longer be zero below the mixed layer, resulting in the vertical propagation of energy. We define the "beating" timescale t_n by

$$t_n = \frac{\pi}{(\omega_n - f)} \tag{3}$$

as the time when mode n becomes out of phase with the high modes at frequencies near f. At this time mode n will contribute to the energy below the mixed layer. Although the details of the energy exchange cannot be explained by this simple argument, it provides a framework for interpreting the model results.

Since ω_n is a function of l, the timescale t_n depends on the initial wavenumber l_0. Smaller-scale disturbances (high horizontal wavenumbers) propagate faster vertically. In an initially southward propagating storm ($l_0 < 0$) the local $|l|$ increases rapidly in time and results in a smaller t_n than $|l|$ for an initial northward propagating storm ($l_0 > 0$), which goes through zero before finally increasing. Hence, the timing of vertical propagation is a strong function of initial wavenumber and is an important point to consider in comparing model simulations and observations.

c. *Horizontal departure of modes*

After $t = 0$ the modes also propagate horizontally. If the initial condition is limited in horizontal extent, the modes will eventually propagate out of the region, with lower modes propagating faster. Initially northward propagating waves will refract at the turning latitude and propagate southward before leaving the area. Locally we define the timescales for mode n to leave due to meridional or zonal propagation by τ_n^{NS} and τ_n^{EW} respectively.

Thus, the propagation timescales τ_n^{NS} and τ_n^{EW} are a strong function of the initial north–south and east–west extents. In general, the smaller the extent of the storm, the sooner the modes leave. When mode 1 leaves, the energy in the mixed layer will decrease. The amount of the decay depends on σ_1, which is determined by the stratification. As mode 1 leaves, the energy below the mixed layer will often increase, as the contribution from mode 1 that was needed to set the initial velocity below the mixed layer to zero will now be absent.

d. *Initial conditions at Ocean Storms*

The initial horizontal wavenumbers generated in the mixed layer during Ocean Storms were estimated from the advection velocity of the atmospheric fronts. The speed C and direction ϑ of the storm were estimated from plots of storm tracks showing the daily position of each front (Lindsay 1988). Crude estimates of the initial wavenumber vector (k_0, l_0) were made for each of the three storm events, where $k_0 = (f/C)\sin\vartheta$, $l_0 = (f/C)\cos\vartheta$ (Table 1). In all three events the storms were propagating to the NE with speeds exceeding 10 m s^{-1}, resulting in initial wavelengths larger than 500 km.

Other estimates of initial horizontal wavenumber were made for the October event by D'Asaro et al. (1995) using surface drifter data to determine the horizontal structure of the mixed layer currents. Their estimates of both k_0 and l_0 ranged near 2.5×10^{-3} km^{-1}, both positive. Although not identical, these values are comparable to those estimated from the storm track (Table 1).

The initial amplitude in the model of the mixed layer current was set to fit the observations.

5. Observations and model comparison

We compare the observations with the modeled response; all three events are discussed together to emphasize differences and similarities. To be consistent in comparing the model results with the observations, the model data were sampled at 47.5°N at the same depths

as the current meters and underwent exactly the same processing as the moored observations. First, we present a general picture of the response by looking at the temporal change of the vertically integrated energy in the mixed layer, pycnocline, and deep ocean. This permits an overall comparison of observations with the model and clearly demonstrates the sensitivity of the model to different initial conditions. Next the detailed vertical structure is examined; at each depth the amplitude and phase of the observations and model are compared. Possible reasons for disagreement between observations and model are explored.

a. Integrated energy comparison

The observed horizontal kinetic energy is shown in the top panels of Fig. 7 for the three events. The vertically integrated HKE of the whole water column (E_T), the mixed layer (E_{ML}), and the pycnocline (E_{PC}) are plotted. Here the pycnocline is defined as the layer from below the mixed layer to 500 m. This definition is based primarily on availability of observations. The mixed layer energy is estimated assuming a constant velocity throughout the mixed layer. The October estimate of E_{ML} from the surface to 35 m is based on nearby surface drifters (D'Asaro et al. 1995a) as there were no current meters in the mixed layer at this time. In January and March the mixed layer extended to 95 and 110 m, respectively, and contained at least two current meters.

After the storm of 4 October the mixed layer energy began to decrease almost immediately, at least by 8 October when the first mixed layer data are available (Fig. 7a$_i$). The decrease was steady until 22 October when virtually no energy remained. Coincident with this decrease was an increase in the E_{PC} that began to rise almost immediately after the storm, reaching a peak on 18 October before decreasing to very low levels by 30 October.

The multiple forcing event of the January storm resulted in a more complicated mixed layer response. Initially E_{ML} increased due to the 12 January event (Fig.

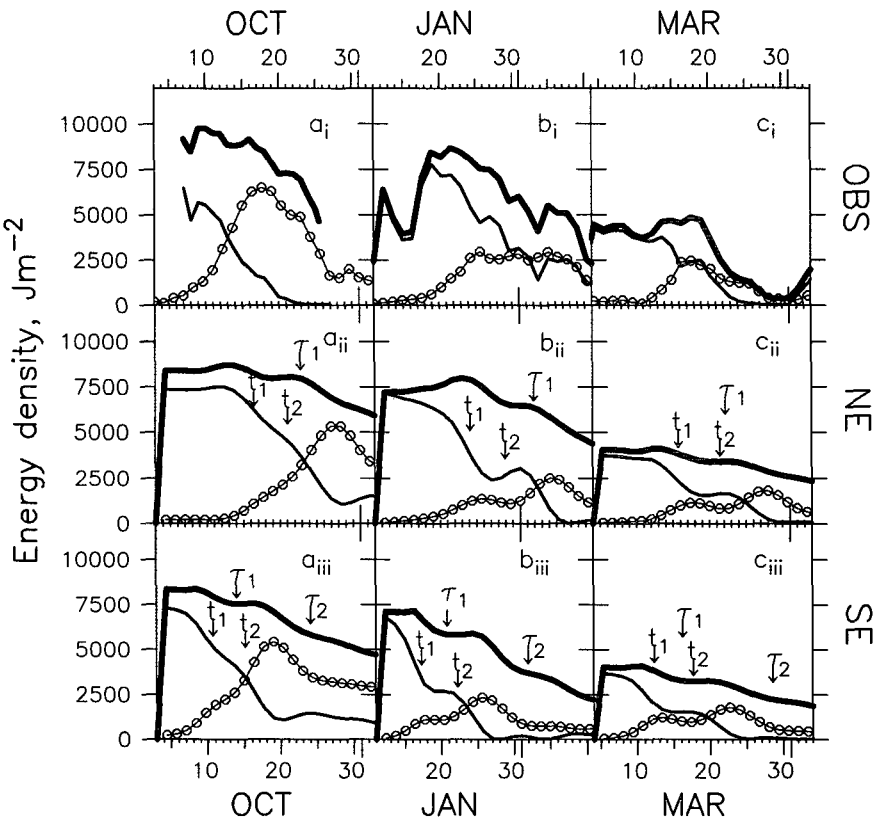

FIG. 7. Vertically integrated HKE of the observations and model as a function of time. Shown are HKE in the mixed layer E_{ML} (light line), the pycnocline E_{PC} (dotted line), and the total depth E_T (heavy line). The observed HKE for the three events are shown in row 1. Corresponding model results are shown below for a front propagating to the NE (row 2) using (k_0, l_0) given in Table 1. The model results for a front propagating to the SE by changing the sign of l_0 is shown in row 3. For labeling, τ_n^{NS} has been abbreviated by τ_n.

$7b_i$). The rapid decay near 15 January was due to additional forcing that added destructively to the existing currents. The large increase during the following few days was apparently due to another forcing event that was nearly in phase with existing currents and added constructively. Unlike the October event, E_{PC} did not increase initially; it took about 8 days before the increase began and 8 more days to reach its maximum value.

After the 5 March event, E_{ML} remained constant for about 9 days before beginning to decrease (Fig. $7c_i$). Similar to the January response the increase in E_{PC} is nearly coincident with the decrease of E_{ML}; E_{PC} peaks 13 days after the event, reaching a maximum of 2500 J m^{-2}, which is 60% of the initial E_{ML} injected by the wind.

During the January and March events, E_T is approximately equal to the sum of E_{ML} and E_{PC}, since nearly all the energy is concentrated in the upper ocean. In contrast, in October there is a significant amount of energy below the pycnocline even before the wind event (Fig. $7a_i$) that obviously came from previous storms. After reaching a maximum in October and January E_T decreased at a rather slow and steady rate. In March E_T remained constant for 15 days before rapidly decreasing.

The corresponding model results for the three events are also shown in Fig. 7. The initial horizontal wavenumber of the mixed layer currents was derived from the storm front velocity as presented in Table 1. The horizontal extent of the storm was assumed to be infinite in the east–west extent and extended 500 km to the north; there was no straightforward way to determine the extent parameters a priori from these observations.

The main features of the model results are similar for the three events, since all events were forced by fronts propagating to the NE. The mixed layer energy remains relatively constant for about 8 days before decreasing. The first significant decrease can be explained by the "beating" of mode 1 (highest frequency) with the higher modes at time t_1.

The magnitude of the decrease of E_{ML} in the model at time t_1 depends on σ_1, the relative contribution of mode 1 to the total solution. At time t_1, E_{ML} will decrease to $(1-2\sigma_1)^2$ of its initial value; the factor of 2 results because mode 1 adds destructively to the other modes in the mixed layer (G84; ZL). The value of σ_1 is ~10% for October, compared to ~20% for January and March (Fig. 6). The difference is due to differences in $N(z)$; there was a shallower mixed layer in October. Thus, we expect the magnitude of the decay of E_{ML} at t_1 to be less for the October event than for the other two events, a prediction certified by the model simulations (Figs. $7a_{ii}$, b_{ii}, c_{ii}). After t_1, E_{ML} continues to decrease coincident with an increase of E_{PC}. Now, a simple explanation using beating modes is difficult as many modes are involved in the solution and the frequency of each mode increases rapidly in time as t^2.

The 8-day delay before the coincident decrease in E_{ML} and increase in E_{PC} observed during the January and March events is reproduced by the model, discounting the more complicated forcing in January. The timing of the October response clearly does not follow the model, with the observed energy beginning to propagate from the mixed layer into the pycnocline almost immediately after the forcing event.

A decrease in E_T in the model can only be explained by a limited horizontal extent of the initial conditions. If the initial extent is infinite, energy can never radiate away. Model runs with limited northern extents of L_N = 250, 500, and 1000 km are displayed in Fig. 8. As expected, the timescale τ_n^{NS} is greater for a longer extent, and the timescale t_n is not a function of extent. At τ_1^{NS}, E_T decreases by a relatively small amount to $(1 - \sigma_1)$ of the initial E_T. By time τ_2^{NS}, E_T is reduced by a factor $(1 - \sigma_1 - \sigma_2)$ of the initial values, which for the three events are factors of 0.7, 0.5, 0.5 respectively. The observed decrease of E_T most closely follows L_N between 250 and 500 km, clearly less than 1000 km. A limited zonal extent would affect the model solution in a manner similar to the north–south extent. We cannot distinguish between finite east–west or north–south extent from the observations, as variations of the parameter L_W have the same qualitative effect as L_N.

In addition to affecting E_T, a limited horizontal extent modifies the time dependence of modeled E_{ML} and E_{PC}. For example, after mode 1 has left the area, energy is reapportioned—decreasing E_{ML} while increasing E_{PC}. Thus, the effective vertical propagation is accelerated. This effect is especially clear at an extent of 1000 km at τ_1^{NS}, where there is a large decrease in E_{ML} coincident with an increase in E_{PC} (Fig. $8a_{iv}$). Since E_{PC} tends to increase at τ_1^{NS}, horizontal extents of less than 250 km (thereby reducing τ_1^{NS}) were tried in order to improve the agreement with observations for the October event. However, agreement between observations and model of the timing of the peak in E_{PC} was not improved significantly.

b. Detailed comparison

The integrated energy provides a useful overall measure to compare model and observations; we now present the complete depth dependence of the observations and model to the three events (Figs. 9a, 10a, 11a). Vectors indicate amplitude (vector length) and phase (vector angle) of the near-inertial horizontal oscillations relative to local f_0; contours of amplitude are also drawn. The wave frequency is related to the change of phase in time; constant phase indicates a pure inertial frequency f_0. The absolute value of phase is of no importance; however, vertical and temporal phase differences are significant. Time series of phase at selected depths are shown in Fig. 12.

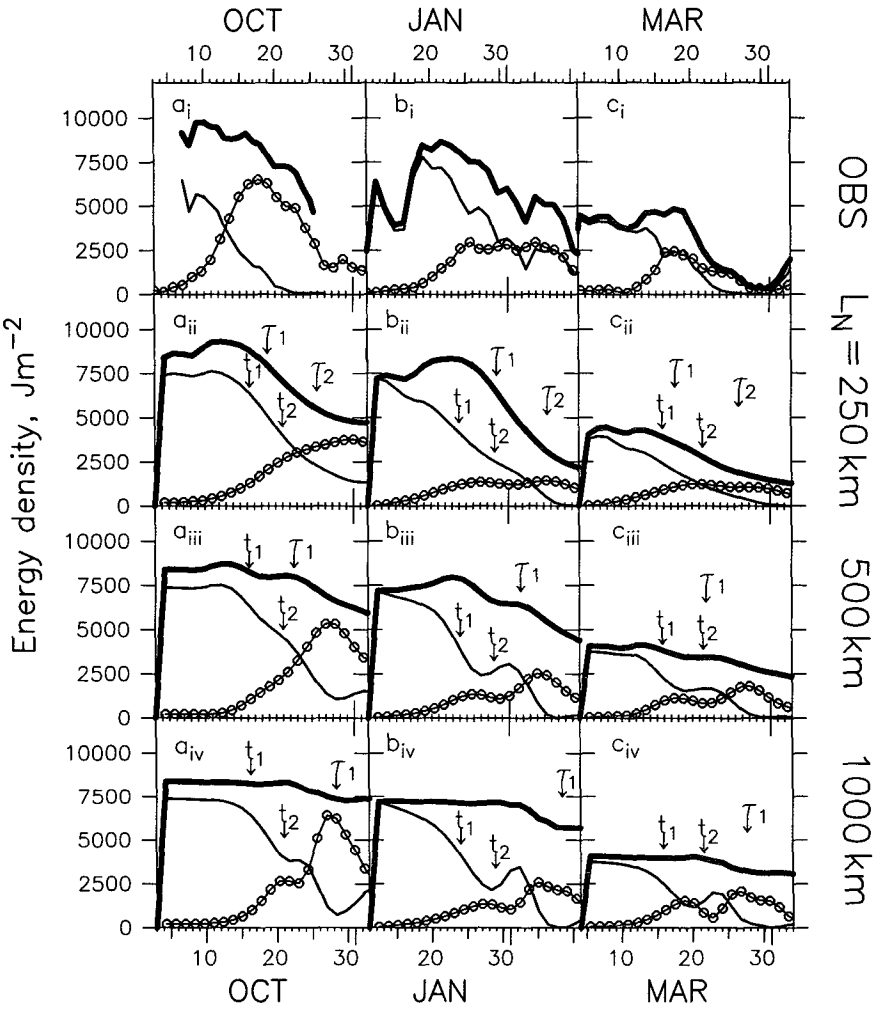

FIG. 8. Vertically integrated HKE of the observations and model as a function of time. Shown are HKE in the mixed layer E_{ML} (light line), the pycnocline E_{PC} (dotted line), and the total depth E_T (heavy line). The observed HKE for the three events are shown in row 1 as in Fig. 7. Corresponding model results are shown below for (k_0, l_0) given in Table 1 with northern extents L_N of 250 km (row 2), 500 km (row 3), and 1000 km (row 4). For labeling, τ_n^{NS} has been abbreviated by τ_n.

The vertical propagation of energy from the October event (Fig. 9a) appears as a well-defined beam of energy that radiates into the pycnocline. As seen in the integrated HKE, the increase of E_{PC} begins immediately after the storm (Fig. 7a$_i$). During the first 10 days the energy increases throughout the pycnocline; after 14 October the energy begins to decrease in the upper pycnocline, creating an energy maximum at 100 m. The maximum weakens as it deepens to 140 m by early November. There is no obvious modulation of the wave amplitude by the stratification. The near-inertial signature of the event is traceable down to at least 1000 m. The observed frequencies are between 1.01 and 1.03 f_0 (Fig. 12) with short periods of lower and even subinertial frequencies. The average frequency increases slightly with depth, resulting in a phase difference between 60 and 195 m that grows in time as the beam propagates deeper. This upward phase propagation is consistent with downward propagating energy in an internal wave (e.g., Leaman and Sanford 1975).

Both the January and March responses appear qualitatively different from the October beam. In contrast to October the energy generated by the storms did not penetrate significantly into the pycnocline for about 8 days. When finally entering the pycnocline, the beam-like structure of the near-inertial energy was not as well defined as in October. The wave field appears to have penetrated to at least 500 m.

In January and March the observed mixed layer frequency remained quite close to inertial, 1.00–1.01 f_0

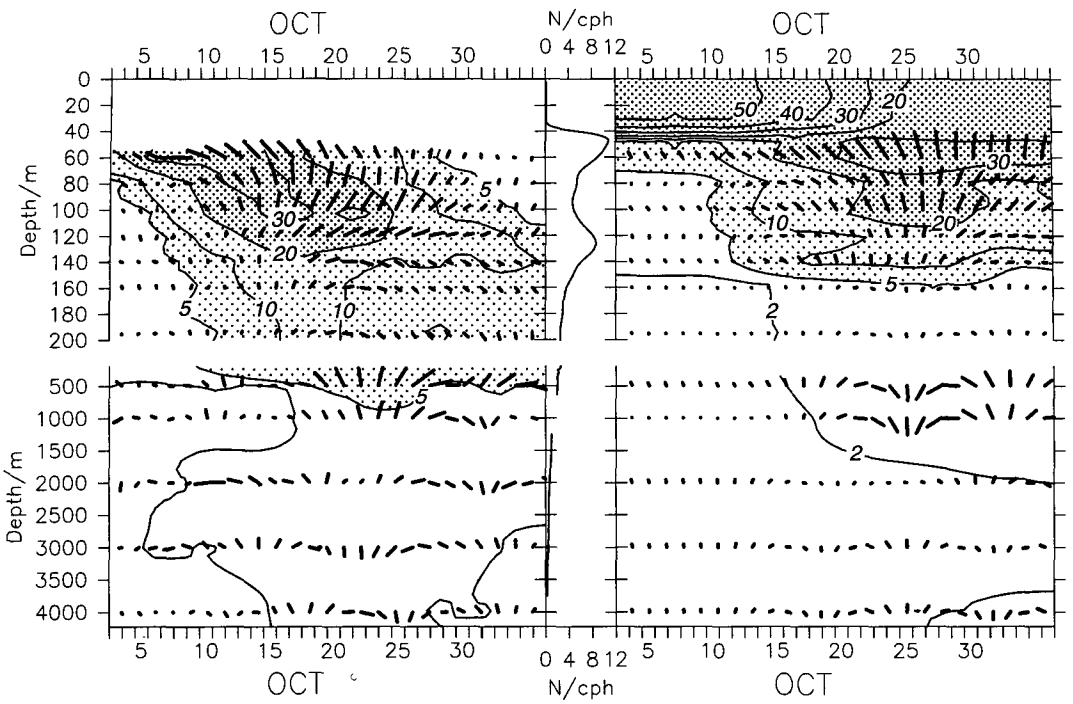

FIG. 9. (a) Observations and (b) model of near-inertial horizontal currents during the October event as a function of depth and time. Sticks represent amplitude (length) and backrotated phase (angle); scale changes below 500 m. Contours of amplitude are also shown. The stratification profile is shown in the center. The model results use (k_0, l_0) given in Table 1.

most of the time (Fig. 12). The vertical structure of the observed phase is also consistent with the downward propagation of energy—constant values of phase propagating upward with time. In both events there are short periods of subinertial frequency followed by periods of high-frequency currents ($1.03-1.05 f_0$) in the mixed layer. The frequency of the pycnocline currents is highest, near $1.05 f_0$, when the amplitude initially increases.

The detailed vertical structure of the model for the three storm events is shown in Figs. 9b, 10b, and 11b. Since all three storms were propagating to the NE, the modeled responses bear many similarities. One characteristic common to all model simulations is that the peak of the wave amplitude propagates very slowly vertically. The energy appears to "stick" at the top of the pycnocline rather than continue to propagate vertically as a beam. The most pronounced difference between model and observation remains the timing of the wave penetration in October: the vertical propagation into the pycnocline occurs almost immediately, unlike the model. In contrast in the January and March events the overall pattern of near-inertial current is reasonably reproduced. In all events the existence of a deep response between 500 and 1000 m is consistent with the model results.

In all events the modeled phase at 60 m is very near $1.01 f$ at least for the first 15 days after the storm (Fig. 12). The phase increases with depth, which is in qualitative agreement with the observations and indicates downward energy propagation. In October the model phase difference between 60 and 140 m increases much slower than the observed; on 25 October the observed phase difference is 135° compared to only 45° in the model. In January and March the observed phase difference across the pycnocline looks more like the model. The model indicates a phase difference of 90° to 135° between the mixed layer (60 m) and 160 m; for the most part this same pattern is seen in the observations.

c. *Discussion*

In the previous sections the comparison between the observed and modeled HKE revealed some similarities and differences in the three events. The events of January and March show considerable agreement between model and data. The October event shows the most striking discrepancy between model and data, as the inertial pumping seems to begin too quickly and E_{PC} peaks too soon. The detailed patterns of amplitude and phase also indicates that the model of the October event does not reproduce the observations very well. To explore possible reasons for the differences, a series of additional model simulations were made to examine the effect of initial wavenumber.

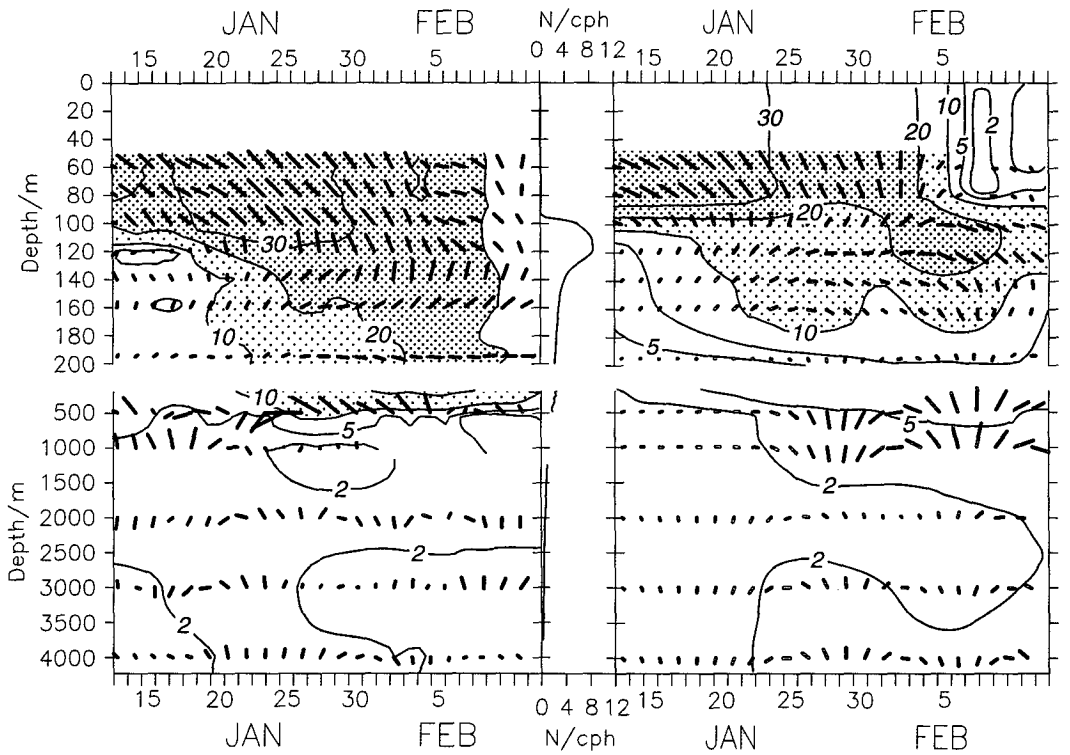

FIG. 10. Same as Fig. 9 but for the January event.

Could slightly different initial conditions alter the model results significantly? As an example, the sign of l_0 was reversed—mimicking a storm front propagating to the SE (Figs. 7a$_{iii}$,b$_{iii}$,c$_{iii}$). In these cases the timescale t_1 is much reduced, resulting in faster propagation from the mixed layer into the pycnocline. This is because smaller-scale disturbances propagate faster in the vertical, and the magnitude of l increases faster if l_0 is negative (1). Clearly the modeled October storm now looks more like the observations. However, SE propagation is not consistent with realistic initial conditions (Table 1) and direct observations of l from a field of drifters in the mixed layer (D'Asaro et al. 1995). For the January and March events the timing of the observed energy exchange between mixed layer and pycnocline is clearly more consistent with storms propagating to the NE than the SE (Figs. 7b$_{ii}$,c$_{ii}$). For a storm propagating to the NE the timescale is typically much longer than a SE storm since the magnitude of l first decreases before finally increasing (1).

The zonal wavenumber k_0 also has an effect on t_1 with larger k_0 (smaller zonal scale) resulting in shorter t_1 and faster vertical propagation. To examine the sensitivity, the timescale t_1 for October is plotted as a function of k_0 for several values of l_0 in Fig. 13. For a NE propagating storm with $l_0 = 6.1 \times 10^{-6}$ m^{-1}, k_0 would have to be a very large value of $\sim 1.3 \times 10^{-5}$ m^{-1} in order to significantly reduce t_1 to 8 days to be in agreement with the October observations. An error in estimating k_0 by a factor of 4 is unlikely, requiring a storm moving slower than 7 m s^{-1}, which is not consistent with the atmospheric data. Direct measurements of k_0 by drifters (D'Asaro et al. 1995) are consistent with $k_0 < 1 \times 10^{-5}$ m^{-1}.

Another explanation for the model discrepancy might be that the relative weights of the first and second modes are incorrect. In October it appears that the peak in the observed E_{PC} as well as the decay of E_{ML} (Fig. 7a$_i$) take place near time t_1 for a NE propagating front (Figs. 7a$_i$, 7a$_{ii}$). Hence, it seems the model would agree better with observations if σ_1 were relatively larger. This might also improve agreement in the January and March events, where the observed pycnocline energy also peaks at time t_1 and is larger than predicted by the model. What would affect the relative weight of mode 1? The value of σ_1 is a function of $N(z)$ and is determined by assuming that the initial current is confined to the mixed layer. However, if the stress penetrated into the pycnocline, the initial current would extend below the mixed layer and might increase σ_1. We performed numerical experiments on the October event extending the initial current 20 m below the mixed layer, but in all of them σ_2 was still larger than σ_1, and

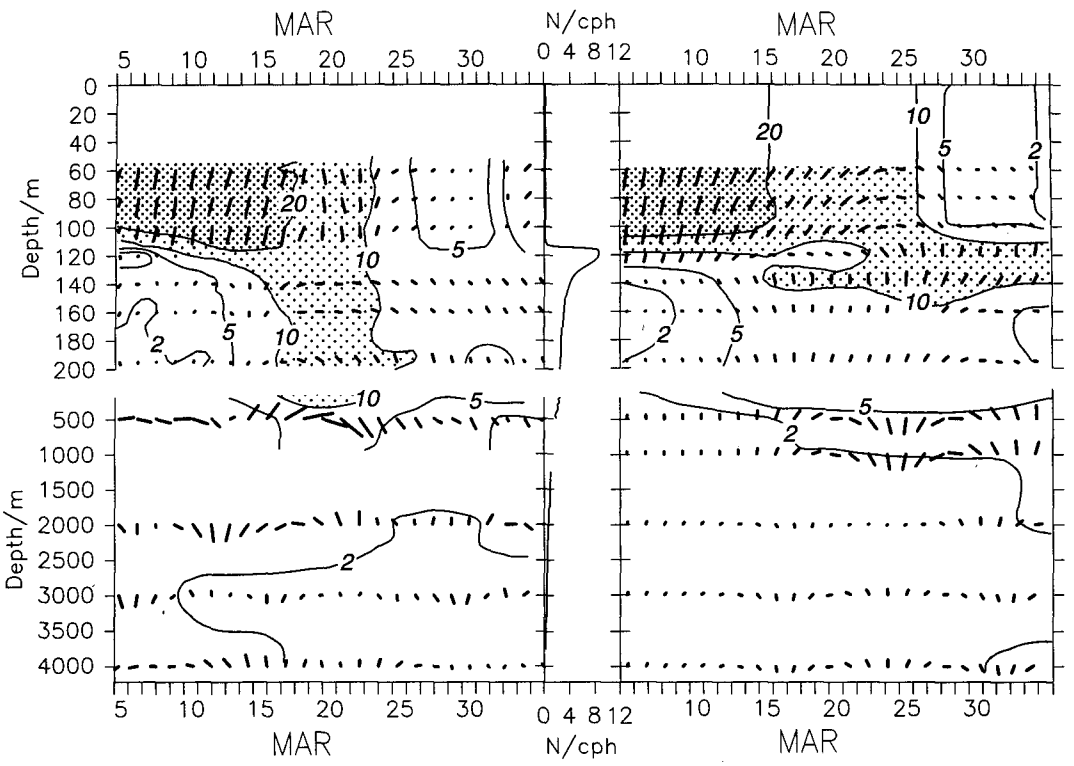

FIG. 11. Same as in Fig. 9 but for the March event.

hence, the resulting modeled wave field still looked more like Fig. 7a$_{ii}$ than the observations (Fig. 7a$_{i}$). Furthermore, the observations indicate that in October the directly forced inertial waves did not extend deeper than 60 m.

Another condition that might affect the vertical propagation of near-inertial motion is the background mesoscale horizontal shear. Investigating this possibility, D'Asaro et al. (1995) compared the spatial scales of the near-inertial field with the low-frequency relative vorticity field, both derived from surface drifter observations. The vertical component of relative vorticity $\zeta \sim 0.2f$ is high enough to affect the horizontal propagation of the near-inertial waves (Kunze 1985) and inertial pumping (Wang 1991). However, D'Asaro et al. (1995) argues that since the near-inertial wave field does not have the same spatial scales as ζ, the evolution of the waves was not dominated by the mesoscale vorticity field. Thus, the interactions of the near-inertial field with the background mean flow does not appear to explain the discrepancy between observations and model in the timing of the inertial pumping. However, given the difficulty in resolving the mesoscale field some effect by the background horizontal shear cannot be ruled out.

The observed currents propagated vertically as a beam, especially in October, while the model results predict a concentration of the current just below the mixed layer. This suggests that in the model the high modes should have smaller amplitudes, or perhaps lose strength in time by some dissipative process. High vertical shears are not present in the data, which also suggests that a turbulent diffusion process may be acting to remove high shear. However, applying one of the various parameterizations of eddy viscosity that depend upon the total energy in the wavefield (e.g., Gargett 1984) is not possible in this model, where each mode is treated independently. As an alternative, we performed some numerical experiments using an ad hoc procedure to mimic a vertical eddy viscosity: the coefficients of the high modes were gradually reduced in time. The idea is, however, consistent with an analytical solution using modes that includes the specific eddy viscosity that is inversely proportional to $N^2(z)$ (e.g., Fjeldstad 1964). In this solution the amplitude of each mode is damped by a coefficient that is inversely proportional to c_n^2. Hence, higher modes would have higher friction coefficients and would be dissipated sooner, the lifetime of each mode increasing with decreasing n. The model results for October using an ad hoc viscosity is shown in Fig. 14. With viscosity the model currents tend to form a beam that is qualitatively similar to the observations. The addition of viscosity has diffused the high currents that were concentrated

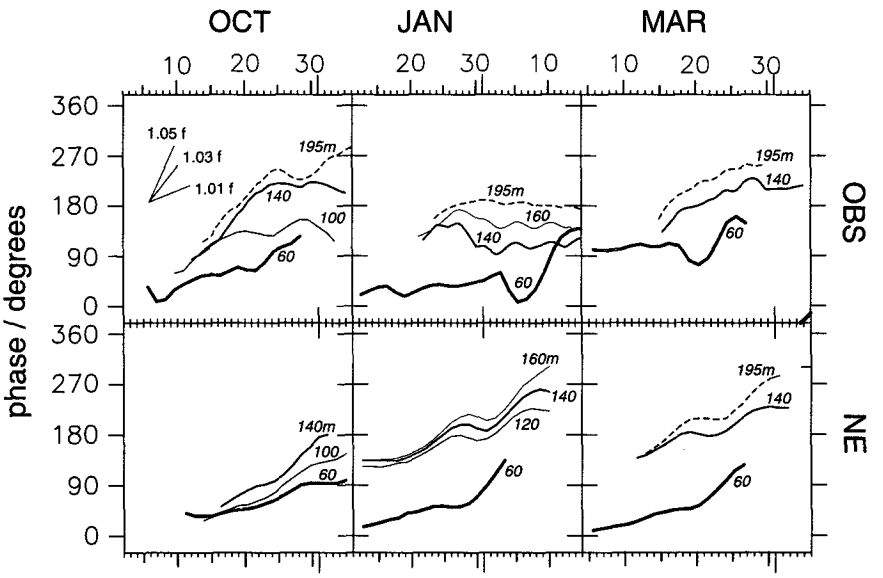

FIG. 12. Time series of backrotated phase of observations (row 1) and model (row 2) for the three events at selected depths. The model results are for a NE propagating front corresponding to row 2 in Fig. 7. Frequency and vertical phase differences can be inferred from this plot. Phase slopes corresponding to frequencies 1.01, 1.03, and 1.05 f_0 are shown.

at the base of the mixed layer. However, the timing of the initial penetration of energy into the pycnocline still fails to reproduce observations. Adding viscosity in the model simulations for January and March did not qualitatively change the comparison between model and observations.

There are other possible factors that might be responsible for the differences between model and ob-

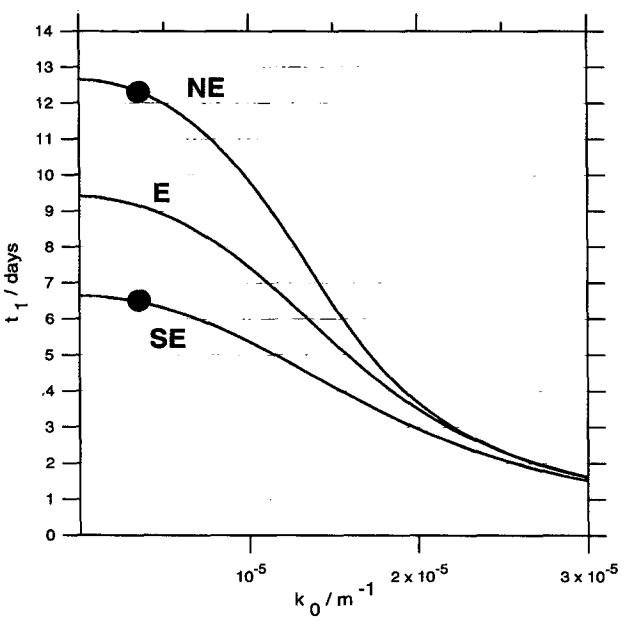

FIG. 13. The timescale t_1 for October as a function of initial zonal wavenumber k_0 for $l_0 = 6 \times 10^{-6}$ (NE), 0 (E), -6×10^{-6} m^{-1} (SE). The dots indicate initial wavenumbers used in the model results shown in Fig. 7 (rows 2 and 3) for October.

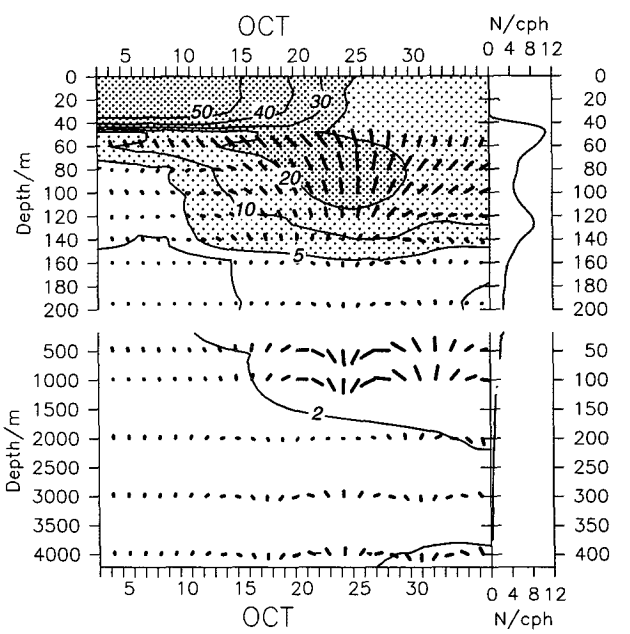

FIG. 14. The model results for the October event as shown in Fig. 9b, but including ad hoc vertical viscosity—eliminating higher modes as a function of time.

servations. Perhaps nonlinear dynamics cannot be neglected. A nonlinear transfer of energy to smaller scales might speed the vertical propagation in October, although it is not clear why nonlinear transfer would be more important in October than the other events. The horizontal scale of the response might not be as simple as modeled. A spectrum of horizontal scales might have been created by variations along the front and changes in frontal speed—these smaller scales would lead to faster vertical propagation. While interesting, assessing the potential importance of these factors is beyond the scope of this paper.

6. Summary and conclusions

This paper compares three distinct events of near-inertial wave generation and propagation observed in the northeast Pacific Ocean during the Ocean Storms Experiment. The observations are compared with results from a linear numerical model. The focus of this investigation is to understand the decay of mixed layer inertial motion due to near-inertial wave propagation into the pycnocline.

As a first step, a slab model, forced by a local wind time series, was used to identify wind events that could generate a significant inertial response (Fig. 1). Three events of strong local forcing were selected for detailed analysis (Figs. 3, 4, and 5): 4 October 1987, 13 January 1988, and 5 March 1988.

Current meter data from a single densely instrumented mooring were filtered to isolate the near-inertial response (Figs. 2, 3, 4, 5). The observed vertical structure of the wave field from each of the events were examined in detail (Figs. 9a, 10a, 11a). A general description of the partition of energy among the mixed layer, pycnocline and deeper ocean was also given (Fig. 7).

A three-dimensional, linear model on a β plane, patterned after G84 and developed in ZL, was run for each of the three events (Figs. 9b, 10b, 11b). The stratification and mixed layer depths used in the model were fit to the background conditions that existed during each event. The model tracks the near-inertial wave propagation that results from a specified initial current structure in the mixed layer. Complete specification of the initial conditions requires giving the amplitude and horizontal structure of the mixed layer oscillations immediately after the forcing. The horizontal wavenumbers of the initial mixed layer currents were estimated from the speed of the atmospheric front (Table 1); the amplitude was set to fit the observations. We explored the dependence of the model on the initial wavenumber magnitude and directions at a range of horizontal extents in order to build a framework for assessing the ability of the model to reproduce observed features of the wave field (Figs. 7, 8). We also relied on the more complete examination of the model as a function of initial conditions given in ZL.

The observed near-inertial response of the three events showed some similarities and some differences:

- The decrease in E_{ML} is coincident with an increase in E_{PC}. The increase in E_{PC} occurred almost immediately after the storm in October, but did not begin for 8 days in January and March (Fig. 7).
- The near-inertial energy appears as a beam in the pycnocline, especially in October. The near-inertial response from each event is traceable down to 500–1000 m (Figs. 9a, 10a, 11a).
- In all events the phase of near-inertial energy propagates upward, consistent with downward energy propagation (Fig. 12).
- The frequency of the waves is typically between 1.01 and 1.05 f_0. The frequency is consistently lower at 60 m (1.01 f_0) and highest in the pycnocline (1.05 f_0) when the amplitude is increasing (Fig. 12).

The comparison between the observations and the linear model showed the following:

- The model shows the initial decrease in E_{ML} is coincident with an increase in E_{PC}—this is consistent with observations (Fig. 7).
- The model predicts E_{ML} is nearly constant for 8 days before decreasing—this is true of all events since the front propagated to the NE. The timing agrees with observations in January and March events, but clearly not in October (Fig. 7).
- The observed amplitude penetrates deeper and appears as a more beamlike structure than in the model, where the maximum currents concentrate at the top of the pycnocline. Despite these differences, the amplitude structure for the January and March events generally agree with the model (Figs. 9, 10, 11).
- The model indicates a deep near-inertial response, reaching between 500 and 1000 m—the observations support this result (Figs. 9, 10, 11).
- In both model and observations the phase increases with depth. However, the observed phase difference across the pycnocline agrees much better with the model for January and March than for October (Fig. 12).

Overall, many features of the January and March events are well represented by the model—modeling of the October event is less successful. The most striking disagreement between observations and model is the timing of the increase in E_{PC} for the October storm. The other two events show a delay of about 8 days before significant energy is transferred from the mixed layer to the pycnocline, which is in reasonable agreement with the model predictions. It appears that processes that are not in the model were important in October. Therefore we investigated some possible effects in an attempt to explain the disagreement in October.

Could the timescale t_1 be shortened by using a different initial wavenumber? This would require the

magnitude of the initial wavenumber to be significantly larger than estimated from the front speed or the propagation direction of the front to be grossly different (Fig. 14). Independent data from drifters (D'Asaro et al. 1995) in the mixed layer suggest the initial conditions used in October were reasonable.

Could a limited horizontal extent, zonal or meridional, affect the timing? A finite horizontal extent results in modes leaving the area. If the horizontal extent is very small, then mode 1 will leave very soon causing an increase in vertical propagation. This effect tends to improve agreement with the observations. However, the contribution of energy to mode 1 (σ_1) is too small to significantly improve the agreement when the extent is shortened.

Could the initial current be deeper than the mixed layer? We ran the model with an initial current that was distributed over a layer deeper than the mixed layer. This increases the relative weight of mode 1 (σ_1), which results in a larger transfer of energy at time t_1. This tends to improve the agreement between the model and observations, since t_1 is about the time when the peak in E_{PC} is observed. This possibility may be especially important in October when the mixed layer is shallow. It appears that a larger proportion of mode 1 would also improve the agreement in January and March. However, no reasonable variation in the thickness of the constant-stress layer improved the agreement significantly.

Could the background relative vorticity increase vertical propagation? Perhaps, but an analysis of a horizontal array of drifters by D'Asaro et al. (1995) suggests that this is not important in October.

Would a vertical eddy viscosity modify the solution significantly? A series of numerical experiments that parameterized viscosity in an ad hoc fashion were tried. The modeled currents showed a more beamlike structure—agreeing better with the observations. However, the timing of the near-inertial model response was not changed with the addition of friction and still fails to reproduce the observed October response.

Clearly, the unforced, linear model fails to adequately predict the timing of the October response, despite considering finite horizontal extent, vertical diffusion of momentum, and variation in initial conditions. If only January and March events were analyzed, the model might be considered a success. What is different about October? The most striking difference is the shallower mixed layer. The stratification and initial conditions determine the modal distributions. Perhaps the wind forcing has created a different partition of energy among the modes than occurs in the unforced model described here. The horizontal scales of the response may be complicated by small-scale variations along the atmospheric front or nonlinear dynamics. Additional observations analyzed in the framework presented here might help identify the most important features missing in the model.

Acknowledgments. We thank Eric D'Asaro for his persistent leadership throughout Ocean Storms. Discussions with Clayton Paulson and Roland de Szoeke are greatly appreciated. Thanks to the Office of Naval Research for their support through Contracts N00014-84-C-0218 and N00014-87-K-0009, and Grant N00014-90-J-1048.

REFERENCES

Bell, T., 1978: Radiation damping of inertial oscillations in the upper ocean. *J. Fluid Mech.*, **88,** 289–308.

Broutman, D., and W. R. Young, 1986: On the interaction of small-scale oceanic internal waves and near-inertial waves. *J. Fluid Mech.*, **166,** 341–358.

D'Asaro, E., 1985: The energy flux from the wind to near-inertial motions in the surface mixed layer. *J. Phys. Oceanogr.*, **15,** 943–959.

——, 1989: The decay of wind-forced mixed layer inertial oscillations due to the beta effect. *J. Geophys. Res.*, **94,** 2045–2056.

——, 1995: Observations and dynamics of the oceanic response to a small-scale storm. *J. Phys. Oceanogr.*, submitted.

——, C. C. Erikson, M. D. Levine, P. P. Niiler, C. A. Paulson, and P. Van Meurs, 1995: Upper-ocean inertial currents forced by a strong storm. Part I: Data and comparisons with linear theory. *J. Phys. Oceanogr.*, **25,** 2909–2936.

De Young, B., and C. L. Tang, 1990: Storm-forced baroclinic near-inertial currents on the Grand Bank. *J. Phys. Oceanogr.*, **20,** 1725–1741.

Eriksen, C. C., 1991: Observations of near-inertial internal waves and mixing in the seasonal thermocline. *Aha Huliko'a Hawaiian Winter Workshop Proceedings,* University of Hawaii at Manoa, 71–88.

Fjeldstad, J. E., 1964: Internal waves of tidal origin. Part I. Theory and analysis of observations. *Geophys. Publ.*, **XXV** (5), 1–73.

Gargett, A. E., 1984: Vertical eddy diffusivity in the ocean interior. *J. Mar. Res.*, **42,** 359–393.

Geisler, J. E., 1970: Linear theory of the response of a two-layer ocean to a moving hurricane. *Geophys. Fluid Dyn.*, **1,** 249–272.

Gill, A. E., 1982: *Atmosphere-Ocean Dynamics.* Academic Press, 346–353.

——, 1984: On the behavior of internal waves in the wakes of storms. *J. Phys. Oceanogr.*, **14,** 1129–1151.

Gonella, J., 1972: A rotary-component method for analyzing meteorological and oceanographic vector time series. *Deep-Sea Res.*, **19,** 833–846.

Greatbatch, R. J., 1983: On the response of the ocean to a moving storm: The non-linear dynamics. *J. Phys. Oceanogr.*, **13,** 357–367.

——, 1984: On the response of the ocean to a moving storm: Parameters and scales. *J. Phys. Oceanogr.*, **14,** 59–78.

Hebert, D., and J. N. Moum, 1993: Decay of a near-inertial wave. *J. Phys. Oceanogr.*, **24,** 2334–2351.

Henyey, F. S., J. A. Wright, and S. M. Flatté, 1986: Energy and action flow through the internal wave field: An eikonal approach. *J. Geophys. Res.*, **91**(C7), 8487–8495.

Koopmans, L. H., 1974: *The Spectral Analysis of Time Series.* Academic Press, 366 pp.

Krauss, W., 1981: The erosion of a thermocline. *J. Phys. Oceanogr.*, **11,** 415–433.

Kundu, P. K., 1984: Generation of coastal inertial oscillations by time-varying wind. *J. Phys. Oceanogr.*, **14,** 1901–1913.

——, 1986: A two-dimensional model of inertial oscillations generated by a propagating wind-field. *J. Phys. Oceanogr.*, **16,** 1399–1411.

——, 1993: On internal waves generated by travelling wind. *J. Fluid Mech.*, **254,** 529–559.

——, and R. E. Thomson, 1985: Inertial oscillations due to a moving front. *J. Phys. Oceanogr.*, **15,** 976–984.

Kunze, E., 1985: Near-inertial wave propagation in geostrophic shear. *J. Phys. Oceanogr.*, **15,** 544–565.

Large, W. G., and G. B. Crawford, 1995: Observations and simulations of upper-ocean response to wind events during the Ocean Storms Experiment. *J. Phys. Oceanogr.*, **25,** 2831–2852.

Leaman, K. D., and T. B. Sanford, 1975: Vertical energy propagation of inertial waves: A vector spectral analysis of velocity profiles. *J. Geophys. Res.*, **80,** 1975–1978.

Levine, M. D., C. A. Paulson, S. R. Gard, J. Simpkins, V. Zervakis, 1990: Observations from the C1 mooring during Ocean Storms in the N.E. Pacific Ocean, August 1987–June 1988. Reference 90-3, Data Report 151, Oregon State University, 156 pp.

Levitus, 1982: *Climatological Atlas of the World Ocean.* Prof. Paper No. 13, National Oceanic and Atmospheric Administration, U.S. Department of Commerce, Rockville, MD, 173 pp.

Lindsay, R. W., 1988: Surface meteorology during ocean storms field program. Tech. Rep., APL-UW TR 8823, Applied Physics Laboratory, University of Washington.

Millot and Crépon, 1981: Inertial oscillations on the continental shelf of the Gulf of Lions—Observations and theory. *J. Phys. Oceanogr.*, **11,** 639–657.

Paduan, J., R. A. de Szoeke, and R. A. Weller, 1988: Inertial oscillations in the upper ocean during the Mixed Layer Dynamics Experiment. *J. Geophys. Res.*, **94,** 4835–4842.

Pollard, R. T., 1970: On the generation by winds of inertial waves in the ocean. *Deep-Sea Res.*, **17,** 795–812.

——, and R. C. Millard, 1970: Comparison between observed and simulated wind-generated inertial oscillations. *Deep-Sea Res.*, **17,** 813–821.

Price, J. G., 1983: Internal wave wake of a moving storm. Part I: Scales, energy budget and observations. *J. Phys. Oceanogr.*, **13,** 949–965.

Rubenstein, D. M., 1983: Vertical dispersion of inertial waves in the upper ocean. *J. Geophys. Res.*, **88,** 4368–4380.

Shay, L. K., and R. L. Elsberry, 1987: Near-inertial ocean current response to Hurricane Frederick. *J. Phys. Oceanogr.*, **17,** 1249–1269.

——, ——, and P. G. Black, 1989: Vertical structure of the ocean current response to a hurricane. *J. Phys. Oceanogr.*, **19,** 649–669.

Smith, S. D., 1988: Coefficients for sea surface wind stress, heat flux, and wind profiles as a function of wind speed and temperature. *J. Geophys. Res.*, **93**(C12), 15 467–15 472.

Tabata, S., L. A. F. Spearing, R. H. Bigham, B. G. Minkley, J. Love, D. Yelland, J. Linguanti, and P. M. Kimber, 1988: STP/Hydrographic Observations along Line P, Line R and Associated Lines and in the "Ocean Storms" Area: Cruise I—22 September–16 October, 1987—Cruise III—24 November–9 December, 1987. Canadian Data Report of Hydrographic and Ocean Sciences, No 70, Institute of Ocean Sciences, Department of Fisheries and Oceans, Sidney, B.C., Canada, 132 pp.

Wang, D. P., 1991: Generation and propagation of inertial waves in the subtropical front. *J. Mar. Res.*, **49,** 619–633.

Zervakis, V., and M. D. Levine, 1995: Near-inertial energy propagation from the mixed layer: Theoretical considerations. *J. Phys. Oceanogr.*, **25,** 2872–2889.